View metadata, citation and similar papers at core.ac.uk

brought to you by CORE

provided by UCL Discovery

© 2016, Elsevier. Licensed under the Creative Commons Attribution-NonCommercial-NoDerivatives 4.0 International
http://creativecommons.org/licenses/by-nc-nd/4.0/

Accepted Manuscript

Tailored mesoporous silica supports for Ni catalysed hydrogen production from ethanol steam reforming

Christopher M.A. Parlett, Ayse Aydin, Lee J. Durndell, Lucia Frattini, Mark A. Isaacs, Adam F. Lee, Xiaotong Liu, Luca Olivi, Rima Trofimovaite, Karen Wilson, Chunfei Wu

PII: S1566-7367(16)30472-1
DOI: doi: 10.1016/j.catcom.2016.12.021
Reference: CATCOM 4890

To appear in: *Catalysis Communications*

Received date: 28 August 2016
Revised date: 15 December 2016
Accepted date: 19 December 2016

Please cite this article as: Christopher M.A. Parlett, Ayse Aydin, Lee J. Durndell, Lucia Frattini, Mark A. Isaacs, Adam F. Lee, Xiaotong Liu, Luca Olivi, Rima Trofimovaite, Karen Wilson, Chunfei Wu , Tailored mesoporous silica supports for Ni catalysed hydrogen production from ethanol steam reforming. The address for the corresponding author was captured as affiliation for all authors. Please check if appropriate. Catcom(2016), doi: 10.1016/j.catcom.2016.12.021

This is a PDF file of an unedited manuscript that has been accepted for publication. As a service to our customers we are providing this early version of the manuscript. The manuscript will undergo copyediting, typesetting, and review of the resulting proof before it is published in its final form. Please note that during the production process errors may be discovered which could affect the content, and all legal disclaimers that apply to the journal pertain.

ACCEPTED MANUSCRIPT

Tailored mesoporous silica supports for Ni catalysed hydrogen production from ethanol steam reforming

Christopher M.A. Parlett,*[a] Ayse Aydin,[b] Lee J. Durndell,[a] Lucia Frattini,[a] Mark A. Isaacs,[a] Adam F. Lee,[a] Xiaotong Liu,[b] Luca Olivi,[c] Rima Trofimovaite,[a] Karen Wilson,[a] and Chunfei Wu*[b]

Corresponding authors

E-mail: c.parlett@aston.ac.uk; Tel: +44 (0)1204 4100 and c.wu@hull.ac.uk; Tel: +44 (0)1482 466464

a. European Bioenergy Research Institute, Aston University, Birmingham, B4 7ET, UK.

b. Chemical Engineering, School of Engineering, University of Hull Cottingham Road, HU6 7RX, UK.

c. Sincrotrone Trieste, ELETTRA, 34012 Basovizza (TS), Italy.

Abstract

Mesoporous silica supported Ni nanoparticles have been investigated for hydrogen production from ethanol steam reforming. Ethanol reforming is structure-sensitive over Ni, and also dependent on support mesostructure; three-dimensional KIT-6 possessing interconnected mesopores offers superior metal dispersion, steam reforming activity, and on-stream stability against deactivation compared with a two-dimensional SBA-15 support.

Keywords

Hydrogen production; ethanol steam reforming; nickel; nanoparticles; mesoporous materials

ACCEPTED MANUSCRIPT

ACCEPTED MANUSCRIPT

Introduction

Rising concerns over availability and accessibility of fossil fuel reserves and the impact of their combustion on climate change is driving research in alternative renewable fuels,[1] which will be vital in meeting legally mandated EU CO_2 emissions targets.[2] Hydrogen derived from biomass, via catalytic steam reforming of bioethanol, is acknowledged as a sustainable production route,[3] with catalyst development key to its successful implementation as a green energy source.

Supported nickel nanoparticles are promising reforming catalysts due to their low cost and earth abundance relative to noble metals,[4] but are prone to deactivation by coking[5] and sintering.[5] Carbon deposition can be mitigated by modifying the reaction conditions, e.g. increasing temperature, water:ethanol ratio or co-feeding O_2, although often at the expense of particle sintering, higher operating costs or undesired Ni oxidation.[6]

Tuning the chemical composition of supports represents an alternative strategy to control coke accumulation; adjusting the acid/base nature by the addition of alkali metal or alkali earth metal promotors disfavours ethanol dehydration and ethylene polymerisation over acidic species.[6] Rare earth and transition metal oxides such as CeO_2 and ZrO_2 exhibit labile surface oxygen, enabling coke oxidation to CO_2.[7] Unfortunately, the low intrinsic surface areas of such reducible oxides can result in poor dispersion of transition metal active sites, while porous analogues suffer from low hydrothermal stabilities, and thus have been co-deposited alongside active Ni phases. [8-10] The deposition of thin films of these oxide has also be implement to curtail these inherent drawbacks.[11]

Silica is commonly utilised as a high surface area, chemically inert support, with both commercial and simple sol-gel synthesised silicas having been employed for Ni catalysed ethanol steam reforming (ESR), with active site dispersion[12] and accessibility,[13] and metal-support interactions[14] (e.g. nickel phyllosilicate formation at the interface[15]) emerging as important factors in regulating activity and deactivation.

Ordered mesoporous silicas, notably SBA-15, SBA-16 and KIT-6, are widely used supports in heterogeneous catalysis, facilitating high dispersions of metal active site with enhanced accessibility.[16] Although a Ni/SBA-15 catalyst has been previously reported for ESR,[8, 9, 17-19] metal sintering and/or coking were observed likely due to the presence of large Ni nanoparticles on the external support surface (rather than in-pore) and led to co-deposition of modifying species. Ni encapsulation, within a

ACCEPTED MANUSCRIPT

protective silica shell[20] has also been shown to be beneficial in overcoming sintering during methane reforming.

Here we demonstrate that Ni nanoparticles can be successfully incorporated within the mesopores of high area silica frameworks, SBA-15[21] and KIT-6,[22] with the resulting materials exhibiting improved catalyst stability and activity for ESR due to confinement of sub-5 nm particles which disfavour undesired methanation side reactions.[23, 24]

Experimental

SBA-15 comprises a two-dimensional hexagonal close-packed assembly of mesopore channels (*P6mm*), whereas KIT-6 comprises a three-dimensional structure of interconnected mesopore channels (*Ia3d*) and were synthesised by the reported methods of Zhao and Ryoo respectively.[21, 22] Ni was incorporated by ethylene glycol assisted aqueous wet-impregnation[25] to give loadings spanning 1-10 wt%, with subsequent calcination at 400 °C for 2 h in air (ramp rate 1°C min^{-1}) followed by reduction at 600 °C for 2 h under flow hydrogen (ramp rate 1°C min^{-1} Hydrogen flow 10 cm^3 min^{-1}). The resulting catalytic families were evaluated for their activity towards Ethanol steam reforming at 600 °C for hydrogen production,[26] with no additional in-situ reduction treatment nor were the catalysts subjected to special storage conditions. Full details of synthetic protocols, characterisation techniques and reaction conditions are reported in the ESI.

Results and Discussion

Low angle XRD reflections (Fig. S1) and nitrogen adsorption-desorption isotherms, exhibiting type 4 isotherms with H1 hysteresis (Fig. S2), characteristic of the parent SBA-15 and KIT-6 structures were observed. Mesopore cell parameters of 10.4 and 21.2 nm, and Brunauer-Emmett-Teller (BET) surface areas and Barrett-Joyner-Halenda (BJH) mesopore diameters of 803 and 833 $m^2.g^{-1}$ and 4.8 and 5.2 nm, were measured for SBA-15 and KIT-6 respectively in agreement with literature reports. Ni incorporation had minimal influence on the support architecture with cell parameters and mesopore dimension comparable to the parent supports (Fig. S3 and S4). BET surface areas decreased with increasing Ni loading (Fig. S5), with SBA-15 exhibiting the greatest loss of 35-45 % (compared to 17-36 % for KIT-6) possibly due to its associated two-dimensional mesostructure and complimentary microporosity.[27, 28] t-Plot micropore analysis permits deconvolution of the meso- and micropore contributions to the internal porosity of SBA-15,[16] and revealed a significant loss of microporosity,

ACCEPTED MANUSCRIPT

presumably via capping of micropore entrances (typically ~0.6 nm) by Ni nanoparticles, accompanied by a smaller decrease in mesoporosity.

High angle annular dark field scanning transmission electron microscopy (Fig. 1 and S6) confirmed retention of both KIT-6 and SBA-15 mesopore architectures following Ni incorporation, and the formation of highly dispersed nanoparticles. Mean particle sizes ranged from 2.1 to 3.7 nm (Fig. S7), similar to literature reports of 3.5 nm for 20 wt% Ni/MCM-41,[25] shows the versatility of the impregnation protocol to produce highly dispersed small nanoparticulate Ni. Lower Ni loadings and the use of interconnected KIT-6 decreased particle size and conversely increased Ni dispersion (Fig. S7),[29] with mean particle diameters for both the KIT-6 and SBA-15 supports considerably smaller than the corresponding BJH mesopore diameters, in contrast to reports for Ni/SBA-15.[9, 30] Wide angle XRD analysis of the Ni phase(s) was hindered by the overlap of NiO[200] and Ni[111] reflections at 43.027° and 44.272° respectively, and NiO[111] at 37.035° with the tail of a broad feature from the amorphous framework silica (Fig. S8). However, peak indexing of the high loading as-prepared materials revealed a mixture of Ni metal and NiO phases, evidenced by X-ray absorption spectroscopy (Fig. S9). Linear combination fitting to nickel standards enabled quantification of the NiO content (Fig. S10), which spanned 97.6 % to 67.8 %, with metallic nickel as the balance. The oxide content was proportional to the Ni dispersion (Fig. S11), in accordance with related studies of SBA-15 and KIT-6 supported Pt[31] and Pd.[32] The observation of significant oxidised Ni (arising during storage under air after reduction) for low loadings (high dispersions) indicates that the ethylene glycol stabiliser was fully removed during the synthesis,[33] consistent with temperature-programmed oxidation (TPO) (Fig. S12) with temperature-programmed reduction (TPR) (Fig. S12) of calcined materials revealing a 600 °C reduction temperature, as used in catalysts preparation, to be sufficient for reduction .

The resulting families of catalysts were subsequently evaluated towards ESR for sustainable hydrogen production.[34] H_2 production was evaluated at 600 °C (with a view to minimize coking) to quantify initial activity and on-stream deactivation (Fig. S13). Mass normalised H_2 productivity averaged over the first 5 min of reaction revealed an inverse correlation with loading (Fig. S14) for both mesoporous supports, mirroring the size-dependent Turnover frequencies (TOFs) for ethanol conversion shown in Figure 2a ; the latter represent a 6 to 10-fold enhancement over similarly prepared 20 nm Ni nanoparticles on commercial silica.[15] Comparison between similar size Ni particles on SBA-15 and KIT-6 reveals similar initial H_2 productivities (Fig. 2b), which are close to an order of magnitude greater than citric acid assisted sol-gel Ni/SiO_2 and Ni/SBA-15 (1375 and 850 $mmol.h^{-1}.g_{Ni}^{-1}$ respectively). [9, 13] The

ACCEPTED MANUSCRIPT

superior activity of the present catalysts reflects their smaller particle size (higher Ni dispersion) and associated genesis of unique active ensembles which presumably feature low coordination sites. Similar structure-sensitivity has also been reported for methanol reforming over Ni/SiO_2 catalysts.[35]

All our Ni/SBA-15 and Ni/KIT-6 catalysts exhibited a common hydrogen selectivity around 69 % (Fig. S15), with CO and CO_2 as the sole other products present in approximately a 1:1 ratio, indicative of a common reforming mechanism which is independent of nickel particle size and support.

Steady state hydrogen productivity for similar sized Ni nanoparticles reveals a significant difference between SBA-15 and KIT-6 supports (Fig. 2 b), with the latter exhibiting excellent on-stream stability. In contrast, the Ni nanoparticles on SBA-15 display significant deactivation, with both H_2 productivity and TOFs (Fig. 3inset) decreasing by ~50 % in under 2 h. Furthermore, the 3.9 wt% Ni/KIT-6 catalyst (possessing 3 nm particles) shows constant hydrogen production over 16 h (Fig. 3). Selectivity towards hydrogen was independent of time on-stream for both supported Ni catalyst families.

The origin of the exceptional Ni/KIT-6 catalyst stability, relative to the rapidly deactivating Ni/SBA-15 materials is intriguing. To elucidate the underlying factor(s), in particular the role of support architecture, spent 4.0 wt% Ni/SBA-15 and 3.9 wt% Ni/KIT-6 catalysts (recovered after 2 h ESR) were characterised. Particle size distributions (Fig. S16) and wide angle XRD (Fig. S17) confirmed that neither suffered sintering, with constant mean particle sizes of 3.2 and 3.4 nm for KIT-6 and SBA-15 respectively. Stability against sintering was further investigated by in-situ XRD of the 4 wt% Ni/SBA-15 (Fig . S17), over an 8-hour period under reducing condition significant nanoparticle growth was not apparent, with only reversible reduction witnessed. Changes in support architecture as the source of SBA-15 deactivation can also be discounted, with STEM (Fig. S16) and low angle XRD (Fig. S17) confirming that the parent framework is preserved post-reaction. However, porosimetry of the spent 4.0 wt% Ni/SBA-15 catalyst reveals a dramatic change in the isotherm hysteresis relative to the as-prepared catalyst, resulting in a 1.2 nm decrease in the average mesopore diameter to 3.6 nm; this is accompanied by a 40 % loss of BET surface area (which falls to 307 $m^2.g^{-1}$). In comparison, the spent 3.9 wt% Ni/KIT-6 catalyst exhibits minimal change in porosity, with the BET surface area only falling by 15 % to 507 $m^2.g^{-1}$. The changing textural properties of the 4.0 wt% Ni/SBA-15 catalyst cannot be attributed to framework contraction and/or pore collapse or Ni particle sintering. Hence, we ascribe deactivation of the SBA-15 supported Ni catalyst to mesopore blockage/narrowing via carbon deposition, consistent with TPO which highlights two new mass losses between 250-500 °C and >500 °C arising from monoatomic and/or amorphous carbon and graphitic carbon respectively (Fig. S19).[36] The three-dimensional interconnected pore

ACCEPTED MANUSCRIPT

architecture of KIT-6 therefore appears less prone to deactivation by coking, and thus more resilient for ESR, with the significantly greater on-stream catalytic stability when employing KIT-6 as the support architecture reflected in its increased level of carbon deposition.

Conclusions

Highly dispersed Ni nanoparticles within mesoporous silica architectures of SBA-15 and KIT-6 exhibit excellent activities towards ESR with high hydrogen selectivity. ESR is structure-sensitive, with H_2 productivity inversely proportional to metal loading/particle size, however selectivity to hydrogen versus CO and CO_2 is size-invariant. The three-dimensional pore network of KIT-6 is superior to the two-dimensional pore network of SBA-15 due to both enhanced dispersion of Ni active sites, and greater resistance towards on-stream deactivation.

Acknowledgements

We thank the EPSRC (EP/N009924/1) for financial support, and Sincrotrone Trieste for the award of XAS beamtime (20155166). We also thank the financial support from Erasmus Internship Program.

References

1. Huber, G. W. and Corma, A., Angew. Chem. Int. Ed., 2007. **46**(38): p. 7184-7201.
2. *http://www.consilium.europa.eu/uedocs/cms_data/docs/pressdata/en/ec/145397.pdf*.
3. Ni, M., Leung, D. Y. C., and Leung, M. K. H., Int. J. Hydrogen Energy, 2007. **32**(15): p. 3238-3247.
4. Guczi, L. and Erdôhelyi, A., *Catalysis for alternative energy generation*. 2012: Springer Science & Business Media.
5. Sehested, J., Catal. Today, 2006. **111**(1–2): p. 103-110.
6. Mattos, L. V., Jacobs, G., Davis, B. H., and Noronha, F. B., Chem. Rev., 2012. **112**(7): p. 4094-4123.
7. Li, S. and Gong, J., Chem. Soc. Rev., 2014. **43**(21): p. 7245-7256.
8. Li, D., Zeng, L., Li, X., Wang, X., Ma, H., Assabumrungrat, S., and Gong, J., Appl. Catal., B-Environ., 2015. **176–177**: p. 532-541.
9. Rossetti, I., Lasso, J., Nichele, V., Signoretto, M., Finocchio, E., Ramis, G., and Di Michele, A., Appl. Catal. B-Environ., 2014. **150**: p. 257-267.
10. Albarazi, A., Galvez, M. E., and Da Costa, P., Catal. Commun., 2015. **59**: p. 108-112.
11. Osatiashtiani, A., Lee, A. F., Granollers, M., Brown, D. R., Olivi, L., Morales, G., Melero, J. A., and Wilson, K., ACS Catal., 2015. **5**(7): p. 4345-4352.
12. Wu, C. and Williams, P. T., Environ. Sci. Technol., 2010. **44**(15): p. 5993-5998.
13. Wu, C. and Williams, P. T., Appl. Catal., B-Environ., 2011. **102**(1–2): p. 251-259.
14. Liu, L. P., Ma, X. J., and Li, J., Int. J. Energy Res., 2014. **38**(7): p. 860-874.
15. Zhang, C., Yue, H., Huang, Z., Li, S., Wu, G., Ma, X., and Gong, J., ACS Sustain. Chem. Eng., 2013. **1**(1): p. 161-173.

ACCEPTED MANUSCRIPT

16. Parlett, C. M. A., Bruce, D. W., Hondow, N. S., Newton, M. A., Lee, A. F., and Wilson, K., ChemCatChem, 2013. **5**(4): p. 939-950.
17. He, S. Y., He, S. F., Zhang, L., Li, X. F., Wang, J., He, D. D., Lu, J. C., and Luo, Y. M., Catal. Today, 2015. **258**: p. 162-168.
18. Vizcaino, A. J., Carrero, A., and Calles, J. A., Fuel Process. Technol., 2016. **146**: p. 99-109.
19. Lindo, M., Vizcaíno, A. J., Calles, J. A., and Carrero, A., Int. J. Hydrogen Energy, 2010. **35**(11): p. 5895-5901.
20. Park, J. C., Bang, J. U., Lee, J., Ko, C. H., and Song, H., J. Mater. Chem., 2010. **20**(7): p. 1239-1246.
21. Zhao, D. Y., Feng, J. L., Huo, Q. S., Melosh, N., Fredrickson, G. H., Chmelka, B. F., and Stucky, G. D., Science, 1998. **279**(5350): p. 548-552.
22. Kleitz, F., Choi, S. H., and Ryoo, R., Chem. Commun., 2003(17): p. 2136-2137.
23. Gao, J., Jia, C., Zhang, M., Gu, F., Xu, G., and Su, F., Cat. Sci. Tech., 2013. **3**(8): p. 2009-2015.
24. Weber, A. P., Seipenbusch, M., and Kasper, G., *S.,* J. Nanopart. Res., 2003. **5**(3): p. 293-298.
25. Qiu, S., Zhang, X., Liu, Q., Wang, T., Zhang, Q., and Ma, L., Catal. Commun., 2013. **42**: p. 73-78.
26. Chen, F., Wu, C., Dong, L., Vassallo, A., Williams, P. T., and Huang, J., Appl. Catal., B-Environ., 2016. **183**: p. 168-175.
27. Pollock, R. A., Walsh, B. R., Fry, J., Ghampson, I. T., Melnichenko, Y. B., Kaiser, H., Pynn, R., DeSisto, W. J., Wheeler, M. C., and Frederick, B. G., Chem. Mater., 2011. **23**(17): p. 3828-3840.
28. Kruk, M., Jaroniec, M., Ko, C. H., and Ryoo, R., Chem. Mater., 2000. **12**(7): p. 1961-1968.
29. Soni, K., Mouli, K. C., Dalai, A. K., and Adjaye, J., Catal. Lett., 2010. **136**(1): p. 116-125.
30. Calles, J. A., Carrero, A., Vizcaíno, A. J., and García-Moreno, L., Catal. Today, 2014. **227**: p. 198-206.
31. Durndell, L. J., Parlett, C. M. A., Hondow, N. S., Wilson, K., and Lee, A. F., Nanoscale, 2013. **5**(12): p. 5412-5419.
32. Parlett, C. M. A., Bruce, D. W., Hondow, N. S., Lee, A. F., and Wilson, K., ACS Catal., 2011. **1**(6): p. 636-640.
33. Yan, J.-M., Zhang, X.-B., Han, S., Shioyama, H., and Xu, Q., .Inorg. Chem., 2009. **48**(15): p. 7389-7393.
34. Dunn, S., Int. J. Hydrogen Energy, 2002. **27**(3): p. 235-264.
35. Mihaylov, M., Tsoncheva, T., and Hadjiivanov, K., J. Mater. Sci., 2011. **46**(22): p. 7144-7151.
36. Padilla, R., Benito, M., Rodríguez, L., Serrano, A., Muñoz, G., and Daza, L., Int. J. of Hydrogen Energy, 2010. **35**(17): p. 8921-8928.

ACCEPTED MANUSCRIPT

ACCEPTED MANUSCRIPT

Figure Captions

Figure 1. Dark field scanning transmission electron micrographs of 0.9 wt% Ni/KIT-6 (left) and 0.9 wt% Ni/SBA-15 (middle) with corresponding particle size distributions (right)

Figure 2. Top(a) size dependent TOFs for Ni/SBA-15 and Ni/KIT-6 series and bottom(b) initial and steady state productivity of 3 nm Ni on SBA-15 and KIT-6

Figure 3. Extended ESR of 3.9 wt% Ni/KIT-6. *inset* loading dependent deactivation of Ni/SBA-15 relative to Ni/KIT-6.

ACCEPTED MANUSCRIPT

ACCEPTED MANUSCRIPT

Figure 1

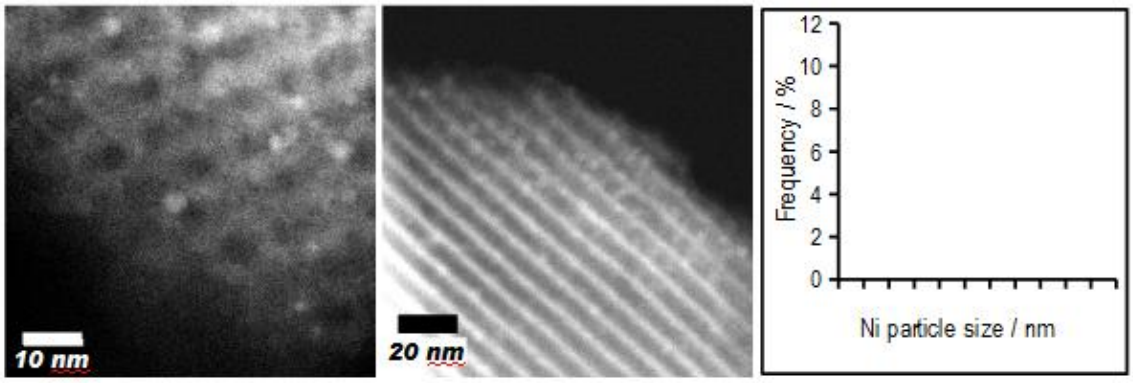

ACCEPTED MANUS

ACCEPTED MANUSCRIPT

Figure 2

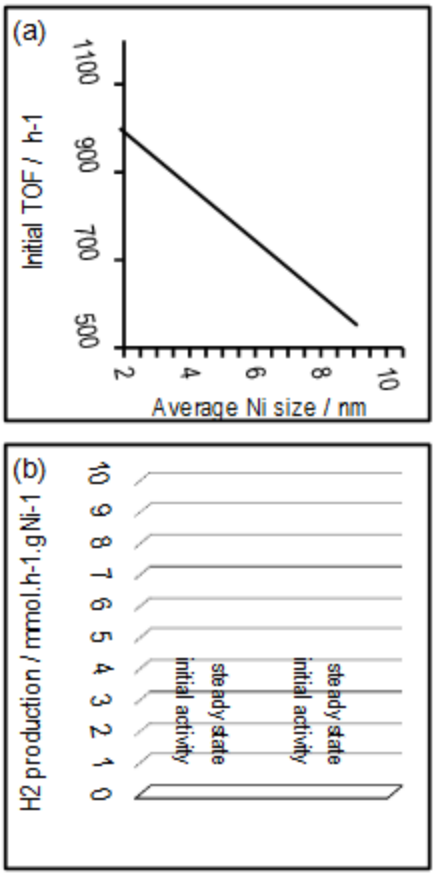

(b)

ACCEPTED MANUSCRIPT

ACCEPTED MANUSCRIPT

Figure 3

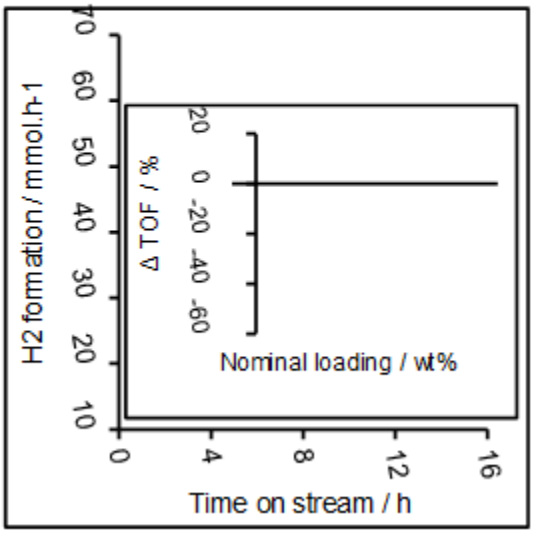

ACCEPTED MANUSCRIPT

ACCEPTED MANUSCRIPT

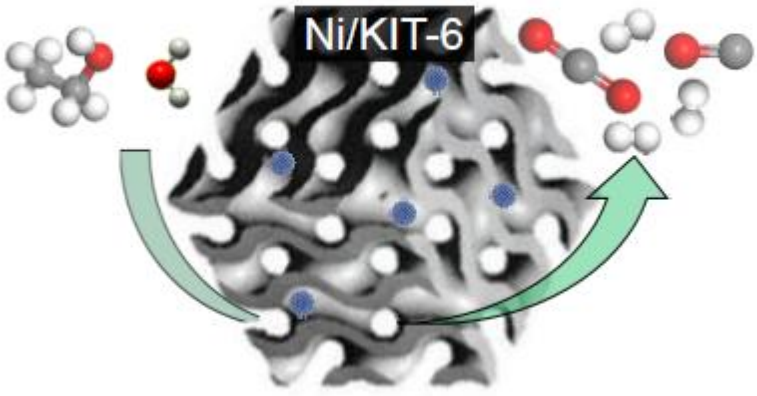

Graphical abstract

ACCEPTED MANUSCRIPT

ACCEPTED MANUSCRIPT

Highlights

- Ethylene glycol assists high active site Ni dispersions within SBA-15 and KIT-6.
- Ethanol steam reforming activity over Ni displays active site structure-sensitivity.
- Three-dimensional architecture of KIT-6 produces stable nickel active sites.
- Coke deposition within two dimensional SBA-15 induces rapid catalyst deactivation.

ACCEPTED MANUSCRIPT